



Contents lists available at ScienceDirect

## Continental Shelf Research

journal homepage: [www.elsevier.com/locate/csr](http://www.elsevier.com/locate/csr)

## Bore collapse and wave run-up on a sandy beach

Erwin W.J. Bergsma<sup>a,\*</sup>, Chris E. Blenkinsopp<sup>b</sup>, Kévin Martins<sup>c,d</sup>, Rafael Almar<sup>a</sup>, Luis P. Melo de Almeida<sup>e</sup><sup>a</sup> CNES/IRD-LEGOS (CNES/CNRS/IRD/UPS) - UMR 5566, 14 Avenue Edouard Belin, 31400 Toulouse, France<sup>b</sup> University of Bath, Research Unit for Water, Environment and Infrastructure Resilience (WEIR), Bath BA2 7YY, United Kingdom<sup>c</sup> LIENSs (CNRS-Université de La Rochelle) - UMR7266, 2 rue Olympe de Gouges, 17000 La Rochelle, France<sup>d</sup> EPOC (CNRS-Université de Bordeaux) - UMR5805, Allée Geoffroy Saint-Hilaire, 33615 Pessac, France<sup>e</sup> Universidade Federal do Rio Grande, Avenida Itália - Carreiros, 96203-900 Rio Grande, RS, Brazil

## ARTICLE INFO

## Keywords:

Bore collapse

Swash zone

Run-up

Swash-swash interaction

## ABSTRACT

Wave run-up on beaches and coastal structures is initiated and driven by collapsing incident bores, this process is often considered to define the seaward limit of the swash zone. It is hence a key feature in nearshore wave processes as extreme run-up can lead to structure overtopping and coastal inundation during storm conditions. In addition, the turbulent nature of incident bores and their collapse suspends and advects sediment, resulting in a highly morphologically dynamic swash zone. The cross shore bore collapse location varies from wave to wave and the process is very limited in both spatial and temporal extent, making direct measurement problematic. This paper presents high spatial-temporal resolution LiDAR field measurements of the evolving free-surface in the surf and swash zone which enable the bore collapse detection for 166 waves. These measurements are used to investigate the link between broken wave properties at bore collapse and wave run-up. Incident bores are identified at the seaward boundary of the LiDAR profiles and tracked through the inner surf and swash zones to the run-up limit. It is found that the vertical run-up height exceeds that which would be expected for a perfect conversion of potential to kinetic energy during bore collapse for 24 % of the bores measured. By returning to an existing ballistic-type model to describe the run-up of individual waves, we show that wave run-up can be divided into three components: the bore collapse, terminal bore celerity and their non-linear interaction. For the present dataset, the contribution of the bore collapse and terminal bore celerity is 26 % and 27 % respectively, while non-linear interactions between the two dominates and account for 47% of the measured run-up. By including the terminal bore celerity, the ability to predict run-up is increased by 30 % with the determination coefficient  $r$  increasing from 0.573 to 0.785. Likewise, the RMS-error for the wave run-up shows an approximately 10 % reduction from 0.325 to 0.295 m.

## 1. Introduction

Incident waves dissipate their energy as they break and propagate in the surf zone as bores. As bores reach the shoreline, the wave form compresses as the wave decelerates and eventually collapses leading to wave run-up on beaches or coastal protection structures. The swash zone is recognized as a highly turbulent region with unsteady, non-uniform flows (Chen et al., 2016). The turbulent flows suspend sediment into the water column leading to sediment transport (Cáceres and Alsina, 2012) and relatively rapid morphological change on sandy (Puleo et al., 2000; Masselink and Puleo, 2006) and gravel beaches (Almeida et al., 2015). Consequently, new insight into processes at the boundary between inner and swash zones are valuable to enhance

understanding of beach hydro and morphodynamics. In this work we focus on the shallowest part of the inner-surf zone, the bore collapse and associated vertical run-up. Furthermore, interaction between consecutive swash events is discussed.

Incident bores in relation to run-up have been studied in scaled laboratories with single bores running up a slope, e.g. Battjes (1974), Hedges and Mase (2004). Field measurements of the swash zone have tended to focus on maximum run-up and the statistical distribution of swash excursions using cameras or run-up wires e.g. Hegge and Eliot (1991), Hughes (1992), Stockdon et al. (2006). More recent field studies (Masselink et al., 2009; Blenkinsopp et al., 2011) have investigated more detailed swash hydro and morphodynamics using a variety of techniques in response to the recommendations of Puleo and Butt

\* Corresponding author.

E-mail address: [Erwin.Bergsma@legos.obs-mip.fr](mailto:Erwin.Bergsma@legos.obs-mip.fr) (E.W.J. Bergsma).<https://doi.org/10.1016/j.csr.2019.01.009>

Received 4 August 2017; Received in revised form 19 December 2018; Accepted 16 January 2019

Available online 18 January 2019

0278-4343/ © 2019 Elsevier Ltd. All rights reserved.

(2006) and Puleo and Torres-Freyermuth (2016) who suggested that measurements of swash on a wave-by-wave basis was key to enhancing understanding.

Whitham (1958) describes bore collapse and run-up on a wave-by-wave basis by applying an analytical mathematical solution of a propagating bore in non-uniform water depth. This analytical solution shows that as bores propagate to shore, they reach a maximum finite velocity ( $U_0$ ) proportional to the local water depth. This velocity is often applied as the starting point for run-up models of individual bores such as the ballistic model of Shen and Meyer (1963). Yeh et al. (1989) calculated  $U_0$  through a classical dam-break problem assuming a perfect conversion of potential to kinetic energy. In the same work it is shown through laboratory experiments that the theoretical value overestimates the measured finite velocity for a single fully developed incident bore, while for undular bores there seems to be a better match between theory and measurements. Baldock and Holmes (1999) recognized that the conversion efficiency varies with the type of bore collapse (undular bores, uniform bores or waves breaking on the beach), assuming that the theory of Whitham (1958) is valid for the different types of bore collapse or wave breaking. In order to take imperfect energy conversion into account, Baldock and Holmes (1999) introduced an energy conversion coefficient  $C$ .

The approaches above do not consider direct bore-bore interactions although sediment transport in the swash zone is thought to be greatly affected by the interaction between consecutive swash events (Hughes and Moseley, 2007; Masselink et al., 2009). Capturing the complexity of such interactions is a major challenge to existing hydrodynamic modelling approaches and introduces significant uncertainty into sediment transport predictions (Blenkinsopp et al., 2011). Few existing studies have directly addressed this phenomenon, though Hegge and Eliot (1991) classified swash-swash interaction into 5 categories; free, over-taking, over-riding, suppressed or composite. Over-taking represents a bore that rides on top of the previous bore. Over-riding and suppressed swash-swash interaction modes are linked through the strength of the backwash. The composite mode consists of more than one of the other modes. Baldock and Holmes (1999) used their swash model to incorporate swash-swash interaction, however in their study the effect of interactions was to translate the location of bore collapse and the actual interaction between consecutive swashes was not explicitly considered. More specific bore interaction-focussed laboratory experiments investigated the interaction of two successive bores (Pujara et al., 2015; Chen et al., 2016) in which the former showed that the degree of swash-swash interaction relates to the solitary wave slope parameter (Grilli et al., 1997). Bore-bore interactions influence the cross shore location of the bore collapse, bore height and advection of sediment into the swash zone, which in turn affect swash-morphodynamics (Alsina et al., 2009). In line with this observation, Alsina and Cáceres (2011) showed that for saturated surf-zones the amount of suspended sediment at the inner-surf, swash zone boundary is independent of offshore wave height, but caused by the combined action of incident swell and swell related long-period water oscillations, for example modulation of wave-wave interaction due to the wave group frequency (Alsina et al., 2018).

This paper focuses on swash run-up observed in the field using a 2D LiDAR. A novel technique to capture and extract the bore collapse and incoming bore celerity from the data is presented and applied to investigate the nature of bore collapse and its importance to wave run-up.

## 2. Method

### 2.1. Study site and data collection

In-situ 2D LiDAR data was collected at Nha Trang beach, on the East coast of Vietnam (Fig. 1) during a 9-day field experiment from 26 November to 4 December 2015. The sandy beach of Nha Trang is situated in a semi-enclosed bay, protected by a group of islands at the Southern part of the bay. The 5 km long stretch of beach is therefore

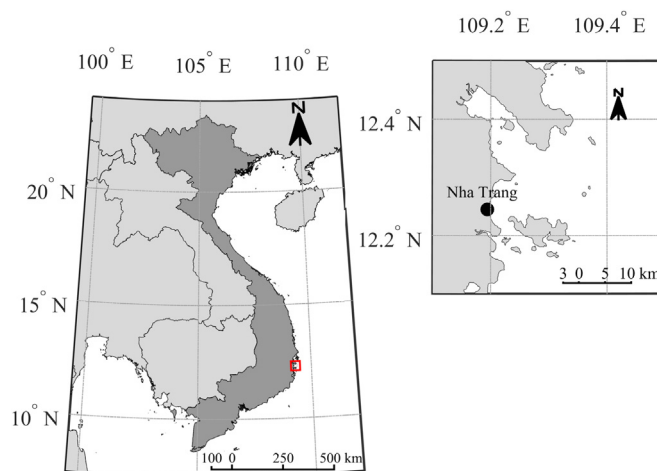


Fig. 1. Left-hand map highlights Vietnam (darker area) and the red square indicates the zoomed area for the right-hand map. The right-hand map shows the location of Nha Trang.

mostly exposed to North-Easterly swell. The East-Vietnam coast experiences a wave climate that is primarily governed by two monsoon seasons; the North East and South West monsoon. The former (latter) is characterized by strong (mild) winds and energetic (moderate) waves. In addition to monsoons, the region experiences occasional tropical storms (typhoons) leading to rapid erosion at Nha Trang bay (Thuan et al., 2016; Almar et al., 2017). During the time-frame of the experiment, the average significant wave height ( $H_s$ ) was 1.07 m, with a corresponding peak period of 11 s. The micro-tidal regime at Nha Trang (maximum tidal range = 1.5 m) consists of a mix of diurnal and semi-diurnal tides (Mau, 2014). The upper beach slope was 0.1 while the inter-tidal terrace has a slope of 0.01. The sediment sizes varies within Nha Trang bay from  $D_{50} = 900 \mu\text{m}$  (coarse) in the North to  $400 \mu\text{m}$  (medium-coarse) in the South (Almeida et al., 2016). During the experiments, almost no wind was present, but this was not measured.

During the field campaign a range of instruments were deployed, an offshore Acoustic Doppler Current Profiler (ADCP), near-shore ADV (Acoustic Doppler Velocimeter), shore mounted video cameras, a swash pole camera, pressure transducers and a 2D LiDAR (for details see Almeida et al., 2016). This paper will focus on data only from the 2D LiDAR which was deployed on a 4 m tall tower above the high tide limit as shown in Fig. 2. LiDAR data was collected at 25 Hz and was typically able to obtain beach profile and free surface data along a transect extending approximately 30 m seaward of the LiDAR position.

The obtained LiDAR data was post-processed using the methodology described by Almeida et al. (2015) and Martins et al. (2016) and interpolated onto a 1D grid with  $\Delta x = 10 \text{ cm}$ . The lower panel in Fig. 2 shows a snapshot of the captured water surface elevation and beach profile data. Here, a 40 min subset of the total collected dataset between 22:21–23:01 on the 27th of November 2015 containing 166 bores is analysed. During this time a significant wave height of 1.2 m and peak period of 12 s was measured offshore.

### 2.2. Bore collapse and vertical run-up

The seaward boundary of the swash zone is characterized by a rapid steepening of the incoming bore and ultimately, as the water depth in front of the bore approaches zero, the bore collapses, driving swash up-rush (Yeh and Ghazali, 1988; Hughes, 1992). As briefly discussed above, previous analytical work by Whitham (1958) suggests that a finite velocity  $U_0$  proportional to the local water depth  $\propto \sqrt{h}$  is reached. It is noted that the empirical approach presented here takes no account of several processes known to influence swash flows, including friction swash-groundwater interactions and porosity e.g. Puleo and Holland

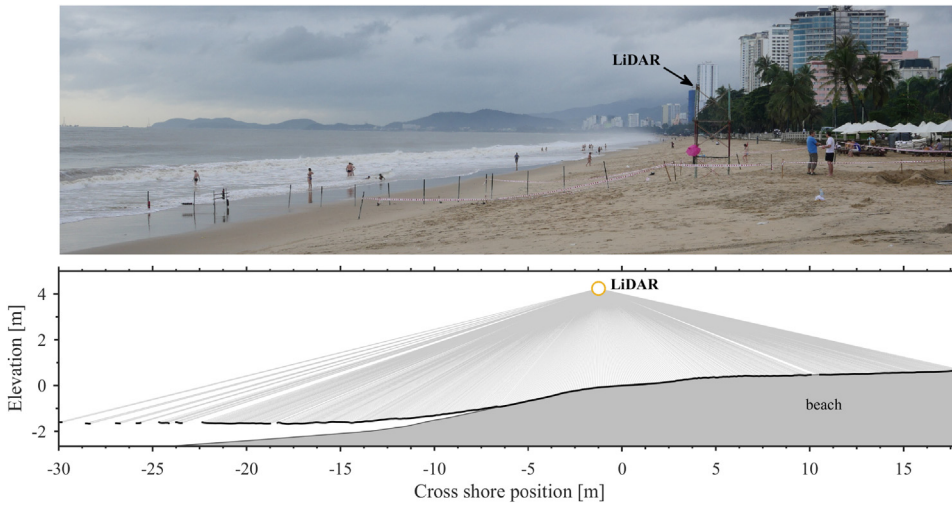


**Fig. 2.** The upper plot shows a photograph of the setup at low-tide at Nha Trang beach during the field experiment. The arrow in the top plot indicates the position of the 2D LiDAR. The bottom plot shows a snapshot of obtained and processed LiDAR data (beach and free surface - black line) at Nha Trang through a schematic representation of the LiDAR position and laser beams.

(2001), Kikkert et al. (2013), Briganti et al. (2013). Yeh et al. (1989) used the classic bore collapse theory to calculate the finite velocity at collapse, assuming a perfect conversion of potential to kinetic energy during the bore collapse process e.g. Baldock and Holmes (1999), Blenkinsopp et al. (2016), Svendsen (2006). This initial shoreline velocity can then be used in to estimate swash trajectory via a ballistic-type model e.g. Shen and Meyer (1963). Hence vertical run-up ( $R$ ) can be approximated as a function of the initial shoreline velocity  $U_0$ :

$$R = \frac{U_0^2}{2g} \quad (1)$$

In which  $g$  is the acceleration due to gravity. The maximum velocity in the case where no energy is lost during the transformation of potential to kinetic energy is approximated as a function of the bore height at collapse following  $U_0 = 2\sqrt{gH_{b,c}}$  (Yeh et al., 1989). Baldock and Holmes (1999) replaced the factor of 2 (perfect conversion) by an empirical bore collapse efficiency coefficient  $C$  to approximate the initial velocity which, in theory, is in the range 1–2:

$$U_0 = C\sqrt{gH_{b,c}} \quad (2)$$

where  $H_{b,c}$  is the bore height at collapse in which according to Shen and Meyer (1963), the bore height must be taken in slope-normal direction. Following (2), the vertical run-up from the bore collapse location can now be calculated as:

$$R = \frac{C^2 H_{b,c}}{2} \quad (3)$$

### 2.3. Detection of bore collapse

The high spatial and temporal resolution of the LiDAR data collected enables individual incident bores to be tracked through the near shore. Tracking of individual bores allows evolving bore characteristics such as bore shape, height, period and the bore collapse process to be captured. The bore tracking methodology is similar to that used in the surf zone by Martins et al. (2016), though instead of tracking peaks in the surface elevation, peaks in its spatial derivative are tracked instead. The tracking was initiated at the cross-shore position  $x = -18$  m. Then, individual bores are subsequently tracked inshore for every  $\Delta x$  by identifying the maximum surface gradient around the previously detected peak. An example of this process is shown in Fig. 3.

Inshore of the breakpoint, the bore front gradient varies considerably in the surf zone with the breaking intensity (Martins et al., 2018). As the bores approach the boundary between inner surf and swash, the front steepens, reaching a local maximum gradient just before the bore collapses (red dot in the bottom plot of Fig. 3). The LiDAR

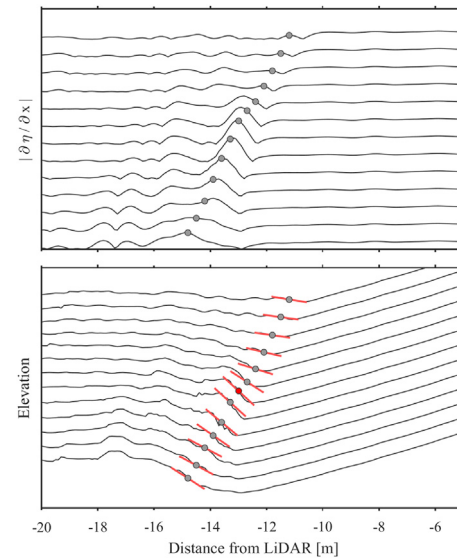


**Fig. 3.** A schematic representation of bore tracking using the LiDAR data. In both plots, the time between every line is 3 time steps ( $\Delta t = 25$  Hz). The upper plot shows the gradient of the measured free surface. The dots represent the tracked bore positions. The dots are the local maximum gradient determined for every gridded cross shore point in time. The lower plot shows the measured free surface elevation and the grey dots are the positions as derived from the upper plot. The red-lines represent the bore front gradient and the red-dot indicates the bore collapse (maximum bore front gradient in time).

is able to detect this and here we define bore collapse as the point at which the local maximum bore front steepness occurs, before the bore front suddenly and rapidly flattens as observed in Fig. 3. Thus the location of bore collapse is defined as the location of the local maximum bore front gradient in time:

$$\text{Bore Collapse} = \max\left(\left|\frac{\Delta\eta_{bf}}{\Delta x}\right|\right)_t \quad (4)$$

In which  $\eta_{bf}$  is the free surface elevation of the bore front which is defined between a seaward and landward limit taken here as:

$$\text{Fitting Limits } \eta_{bf} = \left|\frac{\Delta\eta}{\Delta x}\right| < \frac{1}{8} \max\left(\left|\frac{\Delta\eta}{\Delta x}\right|\right)_t \quad (5)$$

where  $\eta$  is the free surface elevation. In Fig. 4, a dot-dashed line is drawn connecting the points defined by (5) to indicate the bore front slope at collapse. A second line is fitted at the moment of bore collapse

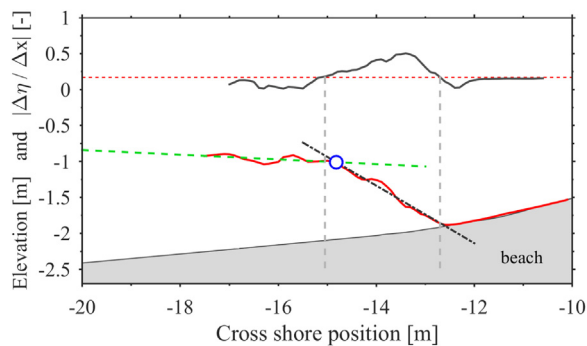


**Fig. 4.** Schematic representation of the bore collapse detection. The solid red line represents the measured free surface elevation, the dash-dotted (–) line is the slope of the bore front, the dashed green line represents the slope of the free surface elevation on the seaward side of the bore head. In the upper part of the plot, the black solid line represents the absolute derivative of the surface elevation and the dashed red line indicates the fitting limit. The grey dashed lines give the used fitting boundaries.

to the free surface elevation 0.5 m seaward of the seaward-limit of (5) as illustrated in Fig. 4. The fitting limits are illustrated by the grey vertical dashed lines in Fig. 4. The intersection of the two lines is taken as the bore head point; indicated by the blue circle in Fig. 4. The bore height is ultimately determined at the bore head point as the vertical distance from the bore head to the bed. The fitting limits used here are calibrated for the current Nha Trang dataset and are therefore site-specific. Nonetheless, considering bore self-similarity, it is expected that similar thresholds are likely to be valid for other datasets with differing site and wave conditions. The same method was used successfully to define surf zone bores by Martins et al. (2018).

The bore height is estimated at every cross-shore location using the surface elevation data. Tracking the incident bores through the surf zone allows for an estimation of the bore celerity. Until bore collapse, changes in the bore shape are minimal, leading to a robust celerity estimate. After collapse, the earlier bore features such as the steep front appear less distinct and as such the celerity estimate is equivalent to the shoreline velocity. At bore collapse, a local bore related Froude number (similar to that presented by Yeh et al., 1989; Zhang and Liu, 2008) based on the bore celerity ( $c_{b,c}$ ) and bore height ( $H_{b,c}$ ) is defined:

$$Fr_{b,c} = \frac{c_{b,c}}{\sqrt{gH_{b,c}}} \quad (6)$$

#### 2.4. Determination of run-up ( $R$ ) from LiDAR data

The run-up of every wave is defined as the distance (horizontal and vertical) between the toe of the bore at collapse and the most landward shoreline position. In order to calculate the vertical run-up ( $R$ ), the shoreline is extracted from the LiDAR data using the 3 cm water depth contours which is tracked throughout the up-rush/backwash cycle.

### 3. Results

#### 3.1. Bore collapse signature from LiDAR

To date, the bore collapse process has predominantly been observed in laboratory experiments and modelled with numerical models (e.g. Yeh et al., 1989; Mory et al., 2011). The LiDAR data provides the opportunity to observe the nature of the bore collapse process on a wave-by-wave basis in the field. An example observation of the most commonly occurring bore collapse sequence is shown in Fig. 5. Fig. 5a shows a bore approaching the shoreline which reaches a maximum steepness at the point of collapse (Fig. 5b). The bore collapse process initiates the swash up-rush (Fig. 5c–d), following flow reversal (Fig. 5e)

the backwash flow is then observed to interact with the proceeding bore (Fig. 5f).

By tracking the bore properties, the spatial development of the bore front gradient can be investigated. Fig. 6 shows the spatial variations of the bore front gradient in the vicinity of bore collapse. At  $x = 0$ , the gradient of the bore front is at its maximum which indicates bore collapse, following (4). The grey lines represent a subset of individual bores from the collected dataset and show the variation in pre/post collapse bore front gradient.

In Fig. 6, the solid blue line shows a relatively stable incoming bore with a bore height of 0.63 m, a terminal bore celerity 1.41 m/s and a Froude number,  $Fr_{b,c} = 0.57$ . The bore front slope at  $x = 0$  m is approximately 17 degrees, 70 % of the maximum steepness at bore collapse. Steepening of the bore front occurs until the bore collapses at  $x = 0$  when the maximum slope ( $\sim 25$  degrees) is reached. Here, the terminal bore front slope angle is in the range of 12–35 degrees which is much flatter than previously observed in the laboratory (Yeh et al., 1989) or in a numerical test case (Mory et al., 2011) which indicated a near-vertical bore front at collapse. After the moment the bore collapses, the collapsing bore slope reduces at a higher rate compared to the steepening observed prior to collapsing. The mean bore front gradient shows that the steepening typically occurs within the last half metre before the bore collapse. This rapid process highlights the need for high spatio-temporal resolution measurements to fully capture bore collapse. The individual bore collapse signatures shown in Fig. 6 highlight the variability of this process.

#### 3.2. Observed bore celerity

Bore celerity through the surf and swash zone can be estimated through the bore tracking methodology. Detection and magnitude of the bore celerity is influenced by changes in bore shape, front slope changes and instabilities. Tracking the bore-head typically over-estimates the celerity as the front steepens. Likewise, tracking the bore toe leads to an underestimate. It was found that the most stable results were obtained by tracking the bore's maximum gradient. Fig. 7 represents the celerity corresponding to the same bores as shown in Fig. 6.

The bore celerity in Fig. 7 is normalised by the minimum bore celerity for each detected wave. Minimum bore celerities are therefore indicated by a value of 1. The blue solid line indicates the estimated celerity for the same bore as highlighted in Fig. 6. Prior to bore collapse, a reduction of the bore celerity can be observed as the bore approaches zero depth. Minimum bore celerity is reached at the point of bore collapse ( $x = 0$ ), where the absolute bore celerity is 1.41 m/s for the highlighted bore. Immediately following bore collapse, a rapid acceleration occurs as the swash flow is initiated (Howe, 2016). The average bore celerity (black dashed line) shows a very similar behaviour with a deceleration prior to the minimum value at bore collapse and subsequent acceleration following the collapse process. The significantly larger error bars after collapse can be explained by the fact that the swash tip is significantly harder to detect due to the flattening of the front (swash-tip) slope and small flow depths.

#### 3.3. Wave run-up

As discussed in the Methods section, previous authors have suggested that the vertical run-up can be considered a function of the bore height at collapse using (3). Fig. 8 shows the vertical run-up as a function of the terminal bore height where the lines indicate constant values of the coefficient  $C$ . It can be observed that the variability of  $C$  is much greater in the current field dataset compared to the large flume experiments described by Blenkinsopp et al. (2016) where values of  $C$  were between 1.95 and 2.25 for monochromatic waves. The average value of  $C$  for the current data is 1.79 with a standard deviation of 0.265, compared to a mean  $\bar{C}$  of 2.09 and standard deviation of 0.08 in Blenkinsopp et al. (2016). Here, we find the majority (75.2 %) of the

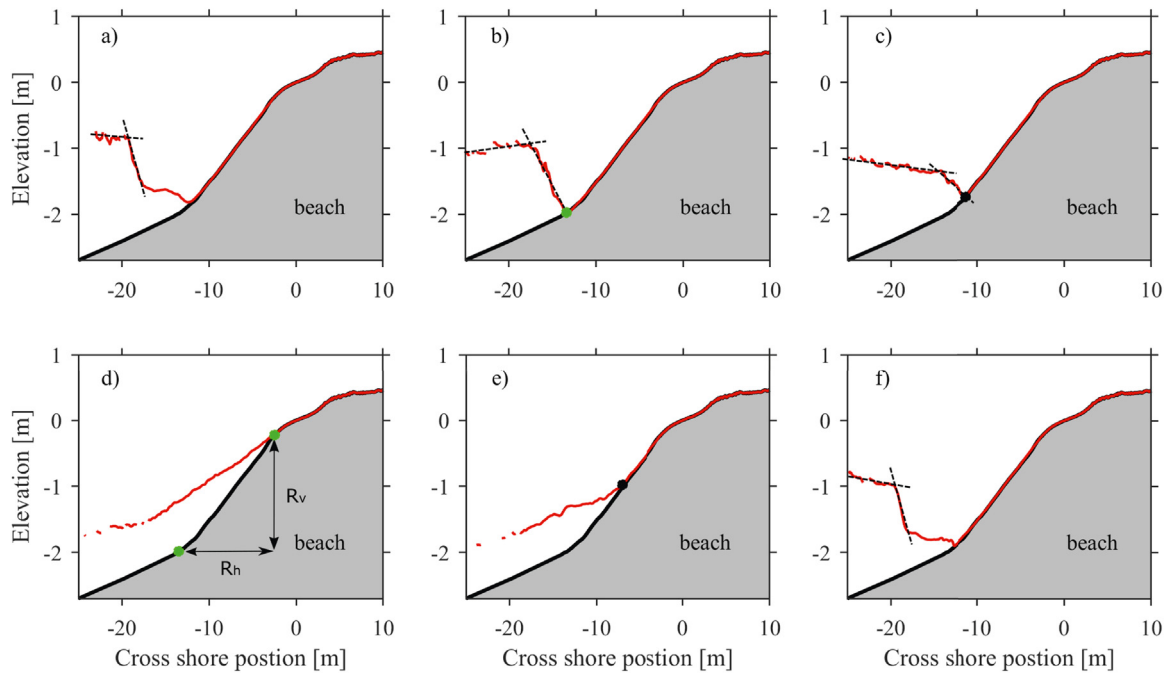


**Fig. 5.** Example of a swash event highlighting the bore collapse process/sequence observed at Nha Trang beach. The sequence shows: a) the incoming bore and the retreating toe of the previous bore 1 s prior to collapse, b) the bore at collapse, c) the initiation of swash motion following bore collapse 1 s post collapse, d) 4 s after the collapse flow divergence between the upper and lower parts of the swash flow, e) latter stages of backwash and f) the arrival of the subsequent bore, 10.5 s after a). The black and green dots indicate the shoreline tracking and the lines the calculated slopes during the collapsing process. Our detection here, mainly focusses on the b)-d) in which the green dots are used to determine the run-down limit at collapse in b) and maximum run-up as the upper green dot in d).

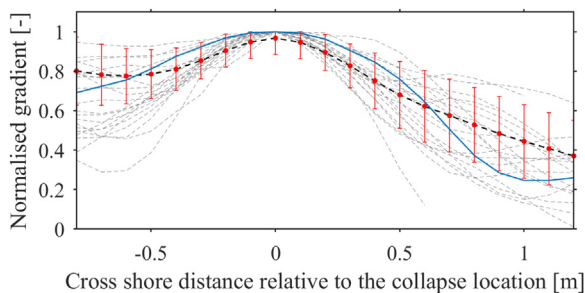


**Fig. 6.** Cross-shore variation of normalised bore front gradient. The grey lines represent the bore front gradient for an arbitrary set of bores. The blue line shows a representative bore discussed in the text.  $x = 0$  is the point of bore collapse. The dashed black line is the mean gradient in space of all observed bores within this dataset and the error bars indicate the associated standard deviation.

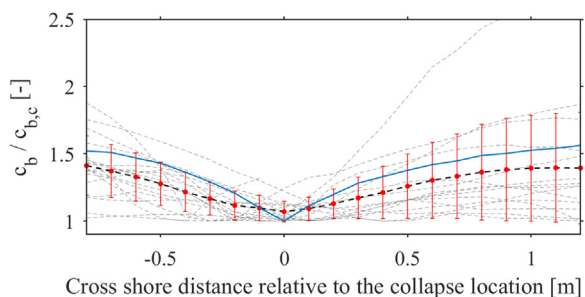


**Fig. 7.** Cross-shore variation of normalised bore celerity (before collapse) and normalised shoreline velocity (after bore collapse). The grey lines represent bore celerity/shoreline velocity for the same bores as in Fig. 6. The blue line shows a representative bore. The dashed black line is the mean bore celerity in space of all observed bores for this dataset and the error bars indicate the associated standard deviation.

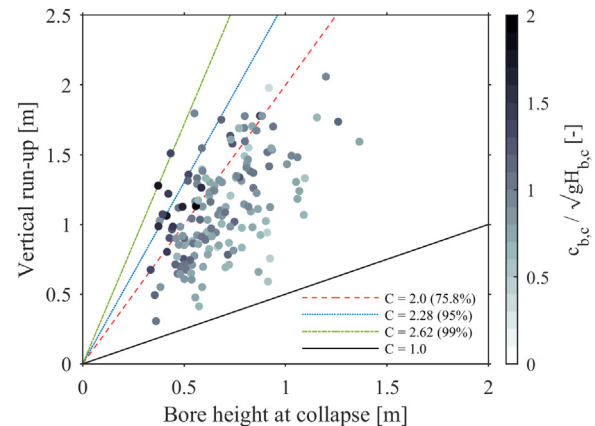


**Fig. 8.** Bore height versus vertical run-up per detected bore collapse. The colour indicates the local bore related Froude number following (6). The lines represent  $C$  thresholds, the red dashed line is  $C = 2$  (perfect conversion), 95% threshold is represented by blue line and the solid green line indicates the 99% interval of the scatter and the theoretical minimum  $C$  ( $C = 1$ ) is represented by the dark black line.

bores have a  $C$ -value indicating an imperfect conversion from potential to kinetic energy ( $C < 2$ ) while a significant portion of the bores experience greater run-up than predicted by Eq. (3) assuming a perfect conversion ( $C = 2$ ). It is suggested that while the bore collapse process is the primary factor in determining initial swash velocity, other processes including swash-swash interaction and terminal bore celerity seem to contribute. Note that  $C$ -values greater than 2 have previously been observed in laboratory experiments with fully developed (Baldock et al., 2009) and solitary bores (Guard and Baldock, 2009).

The dots in Fig. 8 are coloured according to the Froude number at bore collapse defined in (6). It is observed that relatively small values of  $Fr_{b,c}$  tend to correspond to lower values of  $C$  implying that bores arriving with a relatively low celerity tend to generate smaller than

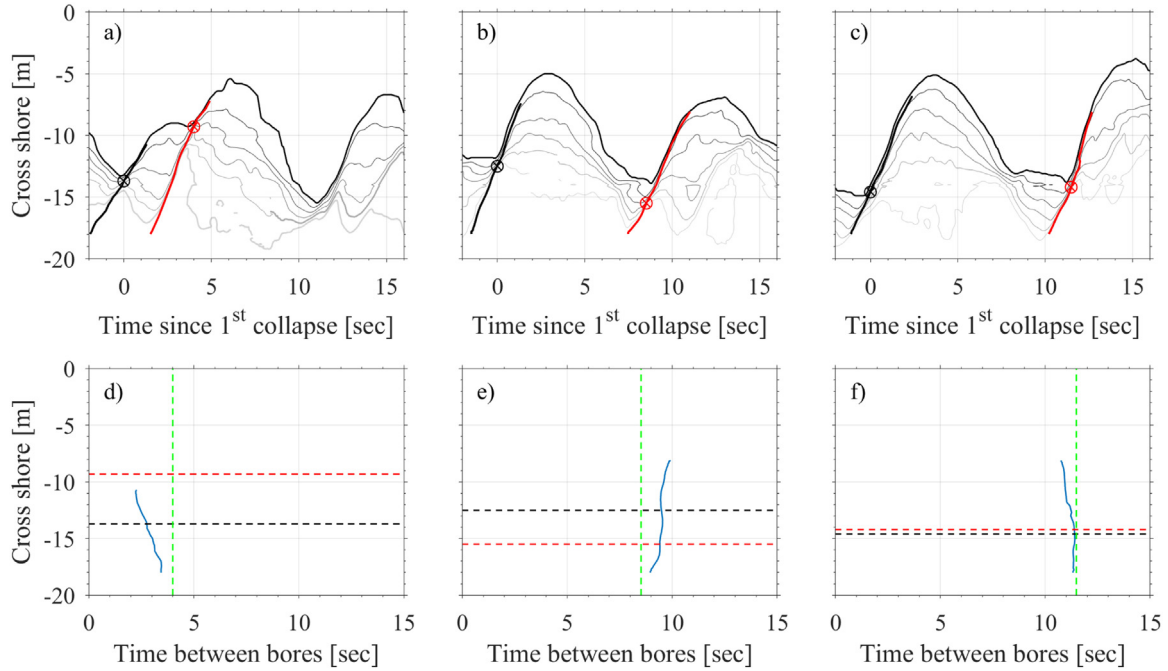


**Fig. 9.** Examples of bore-bore interactions. a) represents an extended run-up due to overtaking, b) indicates a suppressing bore-interaction and c) shows a free swash movement. The black line shows the bore-track of the first incident bore and the red represents the second. The circles represent the detected bore collapse point. d)–f) show corresponding relative time between two consecutive bores as the bores propagate inshore. The black and red dashed lines correspond to the cross shore location of the bore collapse for the first (black) and second (red) bore. The green dashed line represents the time between two consecutive bore collapse events and the blue line shows the time between incident bores propagating inshore.

expected run-up. Observations suggest that such events typically feature strong interaction between the preceding backwash flow and the incoming bore which acts to retard wave run-up. Conversely, relatively large values of  $Fr_{b,c}$  tend to correspond with the higher  $C$ -values, indicating larger than expected run-up for a given bore collapse height. In this case, observations indicate that such events correspond to overtaking swash events according to the definitions of Hegge and Eliot (1991) which act to enhance wave run-up. Over the total dataset 50.3% of the bores are free swashes without bore-bore interaction. 19.3% of the bores are overtaken by the subsequent incident bore (6.2% of the dataset consists of the subsequent bores). Overriding and suppressed bores collectively comprise 16.8% of the total dataset and the remaining 7.4% corresponds to composite swash-swash interactions. While there is clear scatter in measured values of the coefficient  $C$ , if the average measured value (1.79 as found above) is taken to calculate the run-up for each swash event in the dataset using (3), the RMS error is 0.325 m.

The LiDAR data and tracking routines allow individual incident bores and bore-pairs to be tracked, which enables an analysis of bore-bore interactions. Fig. 9 shows 3 example cases with increasing swash duration (hence reducing swash saturation as described in (6)) from left to right: overtaking (a), (partially) suppressing (b) and a free bore (c). In all of the presented cases, the bore heights of two consecutive bores are of similar order at  $-17.5$  m cross shore (seaward of all collapse locations for the presented bores). The maximum difference is 6 cm, which corresponds to 5% of the maximum height of the two consecutive bores. Fig. 9d–f shows the variation in the time between the two consecutive bores as they progress shoreward, and these demonstrate a characteristic behaviour for the different types of bore-bore interaction. For the overtaking case (Fig. 9 a and d), the second bore propagates before the flow reversal of the preceding bore, thus it travels in a greater depth, the bore is partially-advected by the uprush flow and it collapses further landward. As a result, the time between consecutive bores reduces as they move landward, and the maximum run-up is much greater for the second bore despite the fact that the bores had the same height at  $x = -17.5$  m. In the partially suppressing case (Fig. 9 b

and e), the second bore propagates on a seaward-directed backwash flow which holds the bore back prior to collapse, making the bore collapse further seaward and reducing the maximum run-up. The time between consecutive bores reduces in the landward direction due to both a lower terminal velocity and smaller bore collapse height of the second bore. Finally, in the free bore case (Fig. 9 c and f) the bore collapse position of the second wave is almost unaffected by the preceding bore, and the run-up for both bores is very similar

#### 4. Discussion

The results above show a majority of bores with a  $C$ -value smaller than 2. However,  $C > 2$  is found for a significant number of bores which can be important for extrema-analyses such as run-up predictions.  $C$ -values are often greater than predicted by a conversion of potential to kinetic energy during bore collapse and appear to be influenced by the local Froude number. If we assume that the terminal bore celerity  $c_{b,c}$  contributes directly to the initial swash velocity  $U_0$ , we can rewrite (2) as:

$$U_0 = c_{b,c} + \alpha \sqrt{gH_{b,c}} \quad (7)$$

by substituting  $U_0$  using (7) instead of (2) in (1), the vertical run-up can be calculated in terms of the local bore related Froude number (8):

$$R = \frac{[c_{b,c} + \alpha \sqrt{gH_{b,c}}]^2}{2g} \Leftrightarrow R = \frac{[(Fr_{b,c} + \alpha) \sqrt{gH_{b,c}}]^2}{2g} \quad (8)$$

The term in parentheses in the right part of (8) effectively represents  $C$ , which consists of the bore related Froude number and a new conversion coefficient  $\alpha$ , as presented in (9). Considering (9) and by rearranging (3),  $\alpha$  is then related to the run-up and bore height as presented in (10).

$$C = Fr_{b,c} + \alpha \quad (9)$$

$$\alpha = \sqrt{\frac{2R}{H_{b,c}}} - Fr_{b,c} \quad (10)$$

Notably, the definition of  $C$  compared to Baldock and Holmes (1999) has not changed other than that  $C$  is now defined by a celerity component and a conversion efficiency component  $\alpha$  which in the case of a perfect conversion of potential to kinetic energy will take the value 2 as in the earlier formulation (Yeh et al., 1989). Also, the left hand side of (8) allows for a component expansion which suggests that  $R$  is a function of two physical components: terminal bore celerity and the conversion efficiency in the bore collapse process. In addition to these two distinct physical processes, (11) and (12) also include a third term which incorporates non-linear interactions between them:

$$R = \frac{c_{b,c}^2}{2g} + \frac{c_{b,c}\alpha\sqrt{gH_{b,c}}}{g} + \frac{(\alpha\sqrt{gH_{b,c}})^2}{2g} \quad (11)$$

$$R = R_c + R_{\alpha,c} + R_\alpha \quad (12)$$

In (12),  $R_c$  is the run-up component related solely to the terminal bore celerity,  $R_\alpha$  is the component related solely to bore collapse and  $R_{\alpha,c}$  represents non-linear interaction between the terminal celerity and collapse.  $C$  and  $\alpha$  are similar conversion coefficients respectively with and without a terminal bore celerity component. The upper plot in Fig. 10 shows total vertical run-up as a function of the conversion coefficient  $C^2$ . In the lower plot in Fig. 10 the component of the vertical run-up due to the terminal bore celerity  $R_c$  is subtracted from the total run-up, leaving the components of run-up that are related to the terminal bore height at collapse and this is shown as a function of  $\alpha^2$ .

From Fig. 10 it is evident that by removing the component of run-up directly caused by the terminal bore celerity, the relationship between the remaining components of run-up and the bore collapse height is strengthened, as indicated by the reduced scatter. Thus, the results in Fig. 10b indicate the energy converted by the bore collapse process through  $\alpha$ , and the scatter represents the non-linear interaction with the terminal bore celerity. To further highlight this, we present  $R_{\alpha,c}$  and  $R_c$

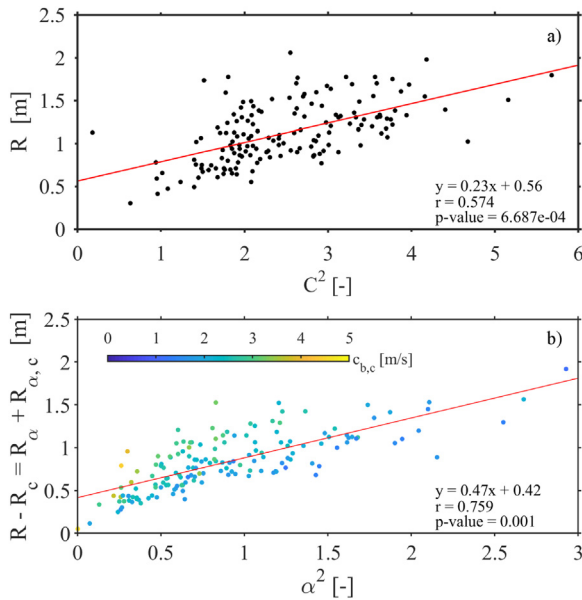


Fig. 10. Scatter plots of run-up versus conversion coefficients  $C$  and  $\alpha$ . a) presents the total run-up as a function of  $C^2$ . b) shows the relation between  $\alpha^2$  and run-up without the terminal celerity component. The colour of the symbols represents the terminal bore celerity. The red lines in both plots represent the linear fit with details presented in the lower right corner of each panel.

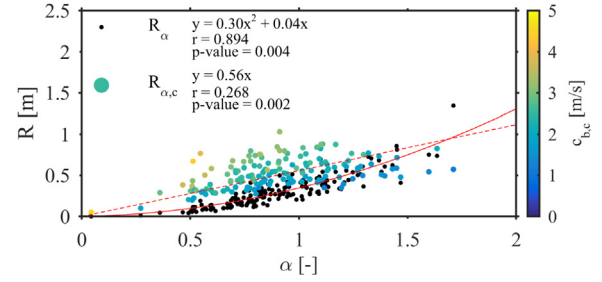


Fig. 11. Scatter plot of  $\alpha$  compared to run-up related to  $c_{b,c}$  and  $\alpha$  represented by the coloured dots  $R_{\alpha,c}$ , whereas the black dots show the run-up related to the energy conversion  $R_\alpha$ . The red lines represent the quadratic fit with between  $\alpha$  and  $R_\alpha$  (solid) and the linear fit between  $\alpha$  and  $R_{\alpha,c}$  (dashed).

as a function of  $\alpha$  in Fig. 11.

Fig. 11 shows that  $R_\alpha$  is smaller than the non-linear interaction term  $R_{\alpha,c}$  for most range of  $\alpha$ , until  $\alpha$  exceeds a value of 1.5. The colouring suggests that even when the value of  $\alpha$  is small, substantial vertical run-up can occur when there is a large value of the terminal bore celerity. It is also evident that the higher values of terminal bore celerity are typically related to low values of  $\alpha$  and for high values of  $\alpha$ , terminal bore celerity tends to be relatively small. For the lower (greater) values of  $\alpha$  this suggests a larger (lower) relative contribution of the terminal bore celerity to the total run-up in comparison to the terminal bore height for the  $R_{\alpha,c}$  term. The solid red line in Fig. 11 represents a quadratic fit to the  $R_\alpha$  component which shows a good and significant correlation to  $\alpha$  ( $r = 0.894$  with an associated p-value of 0.004). Since the non-linear interaction term is also dependent on the terminal bore celerity and non-linear in nature, the correlation with  $\alpha$  is weaker ( $R = 0.268$  and a p-value of 0.002). On average, for all the bores within this dataset, the contribution to the total run-up from  $R_\alpha$  26%, the  $R_c$  term accounts for 27% while the contribution of  $R_{\alpha,c}$  is 47%. This analysis indicates that while the collapse and terminal celerity mechanisms contribute equally to the total run-up, the non-linear interaction term clearly dominates. This highlights the significance of including celerity component to approximate run-up, suggesting that its direct and indirect impact on the run-up and bore collapse process should not be neglected. With the inclusion of bore front celerity, the run-up can be estimated more accurately from measured bore collapse parameters. Using (8) and the average observed  $\alpha$  ( $\bar{\alpha}_{obs} = 0.889$ ) the RMS error for the run-up is reduced by approximately 10% to 0.295 m.

In the previous model by Baldock and Holmes (1999),  $C$  can be seen as a repository of all unknown processes and interactions that occur between the inner surf and swash zone (Svendsen, 2006). A direct link between  $\alpha$  and  $C$  with terminal bore celerity or other measured components was sought to enable improved prediction of individual wave run-up based on measured bore properties. Attempts were made to relate  $C$  and  $\alpha$  to the incident bore front slope, the slope of the free-surface behind the bore front (see green dashed line in Fig. 4) and the relative angle between the two, but no significant relationship could be found other than a weak trend found between back angle and  $C$ . Landward-sloping free surfaces behind the bore front were found to be associated with greater  $C$ -values, while seaward-slope free surfaces behind the bore front tended to have lower  $C$ -values.

## 5. Conclusion

A 2D LiDAR scanner has been used to obtain high spatial and temporal resolution water surface profiles illustrating the complex bore collapse process. From the 2D LiDAR data, it is possible to accurately obtain the bore collapse point in space and time and extract a range of parameters including bore celerity, bore slope and bore height at collapse. It is observed that the terminal bore celerity at collapse is consistently non-zero and the bore collapse front slope is in the range

12–35 degrees to the horizontal.

In agreement with other studies, a clear relationship between wave run-up and bore height at collapse was observed. However, the measurements obtained by tracking incident bores using the LiDAR enabled further analysis of the underlying mechanisms causing wave run-up. This indicates that terminal bore celerity at the point of bore collapse contributes significantly to individual wave run-up and is strongly influenced by bore-bore interactions in the inner surf zone. Term-expansion of an existing ballistic-type model to describe the run-up of individual waves in combination with the novel measurements showed that the total run-up  $R$  could be separated into three different components: bore collapse conversion efficiency, bore celerity and their non-linear interaction. In the dataset presented here, the bore collapse and terminal bore celerity have an equal contribution, while the non-linear interaction between the two dominates the total run-up. This analysis of the driving mechanisms which cause wave run-up, shows that the former conversion coefficient  $C$  can be separated into three components: the bore collapse, terminal bore-celerity and their non-linear interaction. Hence, including terminal celerity with collapsing bores cannot be neglected when investigating or predicting wave run-up at sandy beaches.

### Acknowledgements

The authors would like to acknowledge the financial assistance and funding for E. Bergsma, C. Blenkinsopp and K. Martins through the WAVes into Shallow water (WASH) project provided by the Engineering and Physical Sciences Research Council (EP/N019237/1). The Nha Trang experiment, R. Almar and L-P Melo de Almeida was funded by the French ANR grant (COASTVAR: ANR-14-ASTR-0019). The overall Nha Trang project was funded by Vietnam under the MOST (BKHCN/NDT-HTD/2013/110) and MOST2: NDT.24.FRA.16 agreements. All data created during this research is openly available from the University of Bath Research Data Archive at <https://doi.org/10.15125/BATH-00589>.

### References

- Almar, R., Marchesiello, P., Almeida, L., Hai, T., Tanaka, H., Nguyen, V., 2017. Shoreline response to a sequence of typhoon and monsoon events. *Water* 364 (6), 9.
- Almeida, L., Almar, R., Marchesiello, P., Benschila, R., Martins, K., Blenkinsopp, C., Floch, F., Ammann, J., Grandjean, P., Viet, N., Thuan, D., Binh, L., Sénéchal, N., Detandt, G., Biaisque, M., Garland, T., Bergsma, E., Caulet, C., Tran, H.-Y., 2016. Swash zone dynamics of a sandy beach with low tide terrace during variable wave and tide conditions. In: In proceedings of the XIVèmes Journées Nationales Génie Cotier - Génie Civil, p. 2.
- Almeida, L., Masselink, G., Russell, P., Davidson, M., 2015. Observations of gravel beach dynamics during high energy wave conditions using a laser scanner. *Coast. Eng.* 228, 15–27.
- Alsina, J., Cáceres, I., 2011. Sediment suspension events in the inner surf and swash zone. measurements in large scale and high-energy wave conditions. *Coast. Eng.* 58, 657–670.
- Alsina, J., Falchetti, S., Baldock, T., 2009. Measurements and modelling of the advection of suspended sediment in the swash zone by solitary waves. *Coast. Eng.* 56, 621–631.
- Alsina, J., van der Zanden, J., Cáceres, I., Ribberink, J.S., 2018. The influence of wave groups and wave-swash interactions on sediment transport and bed evolution in the swash zone. *Coastal Engineering* (in press).
- Baldock, T., Cox, D., Maddux, T., Killian, J., Fayler, L., 2009. Kinematics of breaking tsunami wavefronts: a data set from large scale laboratory experiments. *Coast. Eng.* 56, 506–516.
- Baldock, T., Holmes, P., 1999. Simulation and prediction of swash oscillations on a steep beach. *Coast. Eng.* 36, 219–242.
- Battjes, J., 1974. Surf similarity. *Coast. Eng. Proc.* 1, 14.
- Blenkinsopp, C., Masselink, G., Turner, I., Russel, P., 2011. Can standard energetics models be used to predict net cross-shore sediment flux at the beach face? *Aust. J. Civil. Eng.* 9 (1), 16.
- Blenkinsopp, C., Matias, A., Howe, D., Castelle, B., Marieu, V., Turner, I., 2016. Wave runup and overwash on a prototype-scale sand barrier. *Coast. Eng.* 113, 88–103.
- Briganti, R., Torres-Freyermuth, A., Baldock, T.E., Brocchini, M., Dodd, N., Hsu, T., Jiang, Z., Kim, Y., Pintado-Patino, J., Postacchini, M., 2013. Advances in numerical modelling of swash zone dynamics. *Coast. Eng.* 115, 26–41.
- Cáceres, I., Alsina, J., 2012. A detailed event-by-event analysis of suspended sediment concentration in the swash zone. *Cont. Shelf Res.* 21 (6), 1219–1227.
- Chen, B.-T., Kikkert, G., Pokrajac, D., Dai, H.-J., 2016. Experimental study of bore-driven swash-swash interactions on an impermeable rough slope. *Coast. Eng.* 108, 10–24.
- Grilli, S., Svendsen, I., Subramanya, R., 1997. Breaking criterion and characteristics for solitary waves on slopes. *J. Waterw. Port Coast. Ocean Eng.* 123, 102–122.
- Guard, P., Baldock, T., 2009. The influence of seaward boundary conditions on swash zone hydrodynamics. *Coast. Eng.* 56, 506–516.
- Hedges, T.S., Mase, H., 2004. Application of a non-linear shallow water theory to swash following bore collapse on a sandy beach. *J. Waterw. Port Coast. Ocean Eng.* 130, 109–113.
- Hegge, B., Eliot, I., 1991. Swash interactions on sandy beaches. In: *Proceedings of the 10th Australian Conference on Coastal and Ocean Engineering*.
- Howe, D., 2016. *Bed Shear Stress Under Wave Runup on Steep Slopes* (Ph.D. Thesis). University of New South Wales, Australia.
- Hughes, M.G., 1992. Application of a non-linear shallow water theory to swash following bore collapse on a sandy beach. *J. Coast. Res.* 8 (3), 562–578.
- Hughes, M.G., Moseley, A.S., 2007. Hydrokinematic regions within the swash zone. *Cont. Shelf Res.* 27 (15), 2000–2013.
- Kikkert, G., Pokrajac, D., O'Donoghue, T., Steenhauer, K., 2013. Experimental study of bore-driven swash hydrodynamics on permeable rough slopes. *Coast. Eng.* 79, 42–56.
- Martins, K., Blenkinsopp, C., Deigaard, R., Power, H., 2018. Energy dissipation in the inner surf zone: new insights from lidar-based roller geometry measurements. *J. Geophys. Res.: Oceans* 123, 3386–3407.
- Martins, K., Blenkinsopp, C., Zang, J., 2016. Monitoring individual wave characteristics in the inner surf with a 2-dimensional laser scanner (lidar). *J. Sens.* 2016, 11.
- Masselink, G., Puleo, J., 2006. Swash zone morphodynamics. *Cont. Shelf Res.* 26, 661–680.
- Masselink, G., Russell, P., Turner, I., Blenkinsopp, C., 2009. Net sediment transport and morphological change in the swash zone of a high-energy sandy beach from swash event to tidal cycle time scales. *Mar. Geol.* 267, 18–35.
- Mau, L., 2014. *Overview of Natural Geographical Conditions of Nha Trang Bay*. Institute of Oceanography, Nha Trang.
- Mory, M., Abadie, S., Mauriet, S., Lubin, P., 2011. Run-up flow of a collapsing bore over a beach. *Eur. J. Mech./Fluids* 30, 565–576.
- Pujara, N., Lui, P., Yeh, H., 2015. An experimental study of the interaction of two successive solitary waves in the swash: a strongly interacting case and a weakly interacting case. *Coast. Eng.* 105, 66–74.
- Puleo, J., Beach, R., Holman, R., Allen, J., 2000. Swash zone sediment suspension and transport and the importance of bore-generated turbulence. *J. Geophys. Res.* 105, 17021–17044.
- Puleo, J., Butt, T., 2006. The first international workshop on swash-zone processes. *Cont. Shelf Res.* 26, 556–560.
- Puleo, J., Holland, K., 2001. Estimating swash zone friction coefficients on a sandy beach. *Coast. Eng.* 43 (1), 25–40.
- Puleo, J., Torres-Freyermuth, A., 2016. The second international workshop on swash-zone processes. *Coast. Eng.* 115, 1–7.
- Shen, M.C., Meyer, R.E., 1963. Climb of a bore on a beach, part 3 run-up. *J. Fluid Mech.* 14, 305–318.
- Stockdon, H., Holman, R., Howd, P., Sallenger, A., 2006. Empirical parameterization of setup, swash, and runup. *Coast. Eng.* 53 (7), 573–588.
- Svendsen, I., 2006. *Introduction to Nearshore Hydrodynamics*, Advanced Series on Ocean Engineering. World Scientific.
- Thuan, D., Binh, L., Viet, N., Hanh, K., Almar, R., Marchesiello, P., 2016. Typhoon impact and recovery from continuous video monitoring: a case study from nha trang beach, vietnam. In: Vila-Concejo, A.; Bruce, E.; Kennedy, D.M., McCarroll, R.J., (eds.), *Proceedings of the 14th International Coastal Symposium* (Sydney, Australia).
- Whitham, G., 1958. On the propagation of shock waves through regions of non-uniform area or flow. *J. Fluid Mech.* 4, 520–539.
- Yeh, H., Ghazali, A., 1988. On bore collapse. *J. Geophys. Res.* 93 (C), 6930–6936.
- Yeh, H., Ghazali, A., Marton, I., 1989. Experimental study of bore run-up. *J. Fluid Mech.* 206, 563–578.
- Zhang, Q., Liu, P.L.-F., 2008. A numerical study of swash flows generated by bores. *Coast. Eng.* 55, 1113–1134.